Fluorinated Perylene-Diimides: Cathode Interlayers Facilitating Carrier Collection for High-Performance Organic Solar Cells

Jia Yao, Shiyu Ding, Rui Zhang, Yang Bai, Qiuju Zhou, Lei Meng, Eduardo Solano, Julian A. Steele, Maarten B. J. Roeffaers, Feng Gao, Zhi-Guo Zhang, and Yongfang Li**

Organic solar cells (OSCs) have experienced rapid progress with the innovation of near-infrared (NIR)-absorbing small-molecular acceptors (SMAs), while the unique electronic properties of the SMAs raise new challenges in relation to cathode engineering for effective electron collection. To address this issue, two fluorinated perylene-diimides (PDIs), PDINN-F and PDINN-2F, are synthesized by a simple fluorination method, for application as cathode interlayer (CIL) materials. The two bay-fluorinated PDI-based CILs possess a lower lowest unoccupied molecular orbital (LUMO) energy level of ≈−4.0 eV, which improves the energy level alignment at the NIR-SMAs (such as BTP-eC9)/CIL for a favorable electron extraction efficiency. The mono-fluorinated PDINN-F shows higher electron mobility and better improved interfacial compatibility. The PDINN-F-based OSCs with PM6:BTP-eC9 as active layer exhibit an enhanced fill factor and larger short-circuit current density, leading to a high power conversion efficiency (PCE) exceeding 18%. The devices with PDINN-F CIL retain more than 80% of their initial PCE after operating at the maximum power point under continuous illumination for 750 h. This work prescribes a facile, cost-effective, and scalable method for the preparation of stable, high-performance fluorinated CILs, and instilling promise for the NIR-SMAs-based OSCs moving forward.

1. Introduction

In an effort to develop clean and sustainable next-generation energy sources, scientific interest for organic solar cells (OSCs) has been rapidly mounting, as they are physically lightweight and flexible, while being relatively cheap to manufacture and compatible with fast roll-to-roll fabrication.[1,2] As a critical component in OSCs, the cathode interlayer (CIL) between the active layer and the cathode metal plays an important role in improving power conversion efficiency (PCE) and stability of the OSCs.[3,4] Successful CILs have been demonstrated by using organic materials, such as amine-substituted polyfluorene derivative,[5,6] aliphatic amine-containing polymers,[7–9] and non-conjugated small-molecule.[10] Notably, n-type organic semiconductors are attractive options for the CILs, owing to their advantages of relatively high electron affinity and high electron mobility. Therefore, a series of n-type

J. Yao, S. Ding, Y. Bai, Z.-G. Zhang
State Key Laboratory of Chemical Resource Engineering
Beijing Advanced Innovation Center for Soft Matter Science and Engineering
Beijing University of Chemical Technology
Beijing 100029, China
E-mail: zgzhangwhu@iccas.ac.cn

J. Yao, L. Meng, Y. Li
Beijing National Laboratory for Molecular Sciences
CAS Key Laboratory of Organic Solids
Institute of Chemistry
Chinese Academy of Sciences
Beijing 100190, China
E-mail: liyf@iccas.ac.cn

R. Zhang, F. Gao
Department of Physics
Biomolecular and organic electronics
Chemistry and Biology (IFM)
Linköping University
Linköping SE-58183, Sweden

Q. Zhou
Analysis & Testing Center
Xinyang Normal University
Xinyang, Henan 464000, China

E. Solano
NCD-SWEET beamline
ALBA Synchrotron Light Source
Cerdanyola del Vallès 08290, Spain

J. A. Steele, M. B. J. Roeffaers
cMACS
Department of Microbial and Molecular Systems
KU Leuven
Celestijnenlaan 200F, Leuven 3001, Belgium

J. A. Steele
School of Mathematics and Physics
The University of Queensland
Brisbane QLD 4072, Australia

organic materials have been developed for the effective CILs, including functional fullerenes,[11,12] n-doped carbon nanotubes and graphenes,[13] organosilica nanodots,[14] naphthalene diimides (NDIs),[15–19] perylene-diimides (PDIs),[20–28] and osmapentalynes.[29,30] Among them, the PDI-based small molecules stand out for their low synthesis costs and high-performance. Despite the remarkable progress made with the CILs, it is still challenging to design a CIL that is suitable for all the active layers of the OSCs, as the surface energy, electronic properties, and chemical species of the different active layers are largely different. This raises concerns with the interlayer engineering of the OSC.

At present, the PCE of OSCs is being largely improved through the innovation of near-infrared (NIR) absorbing small-molecular acceptors (SMAs), which are distinct from other absorbers due to their significantly lowered lowest unoccupied molecular orbital (LUMO) energy levels, especially when accompanied by halogenation (fluorination or chlorination) substitution.[31] For example, fluorinated SMAs[32,33] (such as IT-4F, IECIO-4F, Y3, and Y6) yield lower LUMO energy levels (≈−4.00 eV or lower) and HOMO (highest occupied molecular orbital) energy levels, relative to their non-fluorinated counterparts (ITIC, IEICO, Y1, and Y5) (Figure S1 and Table S1, Supporting Information). Thus, to minimize the interfacial energy offset in the active layer, polymer donors with deep HOMO energy levels are specifically needed, and fluorinated donors are generally used to fulfill this requirement.[34] The fluorinated materials are thus interesting to tune the energetic properties and aggregation behavior because fluorine is the strongest electron negative atom in nature, being small in size. Recent studies show that fluorination of SMAs can suppress the spin-related pathway of nonradiative loss in OSCs,[35,36] which highlights the importance of the fluorination method in constructing high-performance photovoltaic materials. Thus, the innovation of NIR-SMAs not only results in active layers with high device performance but also leads to different surface energy and electronic properties of the active layers. Moreover, between the active layer and the cathode, an ideal interfacial contact is needed to establish an energy level alignment that favors effective electron extraction and hole blocking.[37] In the NIR-SMAs-based OSCs, the lowered LUMO energy level of the SMAs proposes a new challenge with device engineering for facilitating carrier collection as most reported interlayers have higher LUMO energy levels of ≈−3.7 eV.[20,22] Despite the importance of engineering an energy barrier-free device, few studies have focused on the CIL design in the NIR-NFAs-based OSCs, to enhance electron extraction and improve device stability.

Recently, Zhang et al. reported an aliphatic amine-functionalized perylene-diimide (PDINN) with the advantages of effective work function (WF) tunability, high conductivity, and good interfacial interaction with the active layer, resulting in good device performance.[38] Despite these advantages, we consider that if the LUMO energy level of PDINN (−3.78 eV) could be further lowered to ensure a barrier-free contact, the electron extraction process in the device can be further optimized, making it more suitable as CIL for the NIR-SMAs-based OSCs. As mentioned above, fluorination has been established as a highly efficient way to improve the device performance of OSCs.[35,36,39] Despite the advantages of fluorination, this strategy has not been fully investigated within the CILs, especially in the non-fullerene OSCs. If successful, the surface energy, electronic properties, and stability can be desirably regulated. In addition, substitution on the bay-position of the PDI molecules has proven to be an effective method to modify the energy levels of PDI-based molecules.[40] Therefore, we propose the fluorination of the bay-position of the PDI core to optimize the LUMO energy level for better energy level alignment at the cathode interface. With a new fluorination protocol, two fluorinated derivatives of PDINN, namely PDINN-F and PDINN-2F, are reported. They exhibit much lower LUMO energy levels (−4.08 eV for PDINN-F and −4.00 eV for PDINN-2F), while retaining the advantages of PDINN, such as the outstanding ability to modify the WF of the cathodes and good solubility in methanol. The LUMO energy level of PDINN-F is below that of the BTP-eC9 acceptor (−4.05 eV), leading to a barrier-free electron extraction. Using a modified cathode of PDINN-F/Ag, a high PCE of over 18% has been achieved in the OSCs with PM6:BTP-eC9 as the active layer. In addition, the operation stability of the device is also improved by using the PDINN-F CIL, owing to the suppression of trap-assisted recombination at the cathode interface.

2. Results and Discussion

2.1. Material Synthesis

Fluorine atom has the strongest electronegativity and the substituted fluorine atoms on organic molecules show strong non-covalent interactions (hydrogen-bonding). And the fluorination of arenes is a highly effective approach toward regulating their optoelectronic properties.[31] However, the method for the fluorination is still limited, especially for the n-type organic semiconductors, such as the PDI derivatives. Generally, fluorinated PDI is obtained via a "Helax" reaction,[41] that is, the halogen (chlorine or bromine) exchange with fluoride anions (KF or ammonium fluoride). The slow kinetics consumption is one noticeable limitation of this method. In addition, the reaction is not easily scaled up to obtain the halide precursor, due to the poor selectivity of the perylene core halogenation as well as the dangerous quenching of large excesses of bromine or chlorosulfonic acid. In contrast, nitration is much more selective thanks to the electron-withdrawing character of the nitro group. In addition, the nitration can be carried out at room temperature with the advantages of short reaction time, high yields, and an inherent ability to scale up. Interestingly, we found that while using the nitro-precursor instead of the aryl halides, the fluorination can perform smoothly and complete within only 15 min. With this straightforward and original methodology, here, we proposed a facile, cost-effective, and scalable method for the preparation of fluorinated PDIs for CILs.

The synthetic route of the fluorinated PDIs is depicted in **Figure 1**a, which offers good yield (>80%) and gram-scale production for each step. Experimental details and characterization data are provided in Supporting Information. The tetraester **2** can be easily obtained from the dianhydride **1**, and was subsequently nitrated under mild conditions to obtain the bay-substituted mono-nitro derivative **3** or bis-nitro derivative **4**. Remarkably, the dinitro precursors can be easily converted

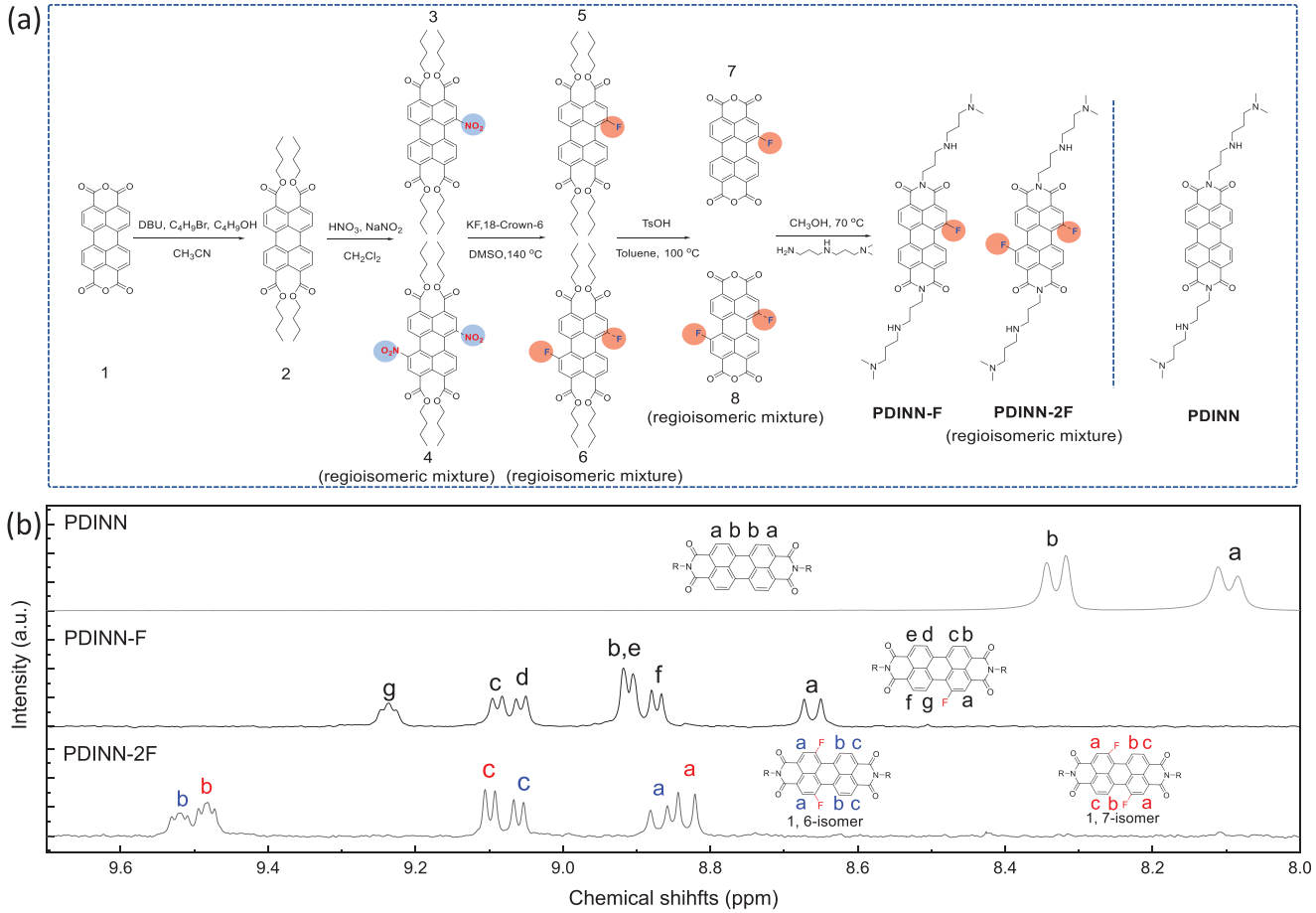

Figure 1. a) Synthesis routes for PDINN-F and PDINN-2F, along with the chemical structure of PDINN. b) An expanded view in the low fields of ^{1}H NMR spectra recorded from the aromatic protons of PDINN-F, PDINN-2F in CD_3OD, and PDINN in CD_3Cl.

to their corresponding fluorinated precursors within 15 min. The analysis of ^{1}H NMR data reveals that the bis-nitration reaction afforded a regioisomeric mixture of 40% of **4**-(1,6) and 60% of **4**-(1,7), the molar ratio of which can be further confirmed by the ^{19}F-NMR of the monomer **6**. The heating of the bay-fluorinated tetraesters in the presence of *p*-toluene sulphonic acid monohydrate yielded the respective anhydrides. Both PDINN-F and PDINN-2F can be easily prepared by condensation of *N,N*-dimethyldipropylenetriamine with the fluorinated perylene dianhydride (**7** or **8**) in methanol and in presence of acetic acid. Starting from dianhydride **1**, the overall yields for PDINN-F and PDINN-2F are 66% and 45%, respectively. The chemical structures of PDINN-F and PDINN-2F were verified by mass spectrometry and NMR spectroscopy (Figures S23, S24, and S25, Supporting Information, for PDINN-F; Figures S26, S27, and S28, Supporting Information, for PDINN-2F). Similar to PDINN, the two fluorinated derivatives show good solubility in methanol, which provide orthogonal solvent processability for CIL film deposition. The bay-fluorinated chemical structures were verified by the ^{1}H NMR spectroscopy (Figure 1b). For PDINN-2F, the assignment of the aromatic protons to the individual 1,7- and 1,6-isomers is also provided in Figure 1b, which is consistent with the proposed chemical structure.

Notably, in the synthesis process of the fluorinated PDIs, adding acetic acid during the final reaction is necessary to prevent the nucleophilic substitution of the amine with the fluorine atom. As a result, the adding acetic acid inevitably leads to the protonation of the polar amine groups attached to the PDI core, as evidenced by the acetyl proton signal at 1.93 ppm for PDINN-F and at 2.12 ppm for PDINN-2F in ^{1}H NMR (Figure S2, Supporting Information). Moreover, further evidence was given by the higher binding energy peak at 402.7 eV from the protonated nitrogen atom in X-ray photoelectric spectroscopy (Figure S3, Supporting Information).[8] From the ratio of integrated peak areas of acetyl proton to aromatic protons, it is suggested that there are two acetic acid molecules in PDINN-F and four acetic acid molecules in PDINN-2F. This was further confirmed by thermogravimetric analysis (TGA) (Figure S2, Supporting Information), with the weight loss of ≈16% corresponding to the loss of two acetic acid molecules in PDINN-F and with the weight loss of ≈26% corresponding to the loss of four acetic acid molecules in PDINN-2F.

To clarify the effect of fluorine substitution on the electronic structure of the PDINN derivatives, density functional theory calculations using the B3LYP functional and the 6-311G(d,p) basis sets were carried out.[42] To simplify the calculations, the acetates were not considered. As shown in Table S2, Supporting

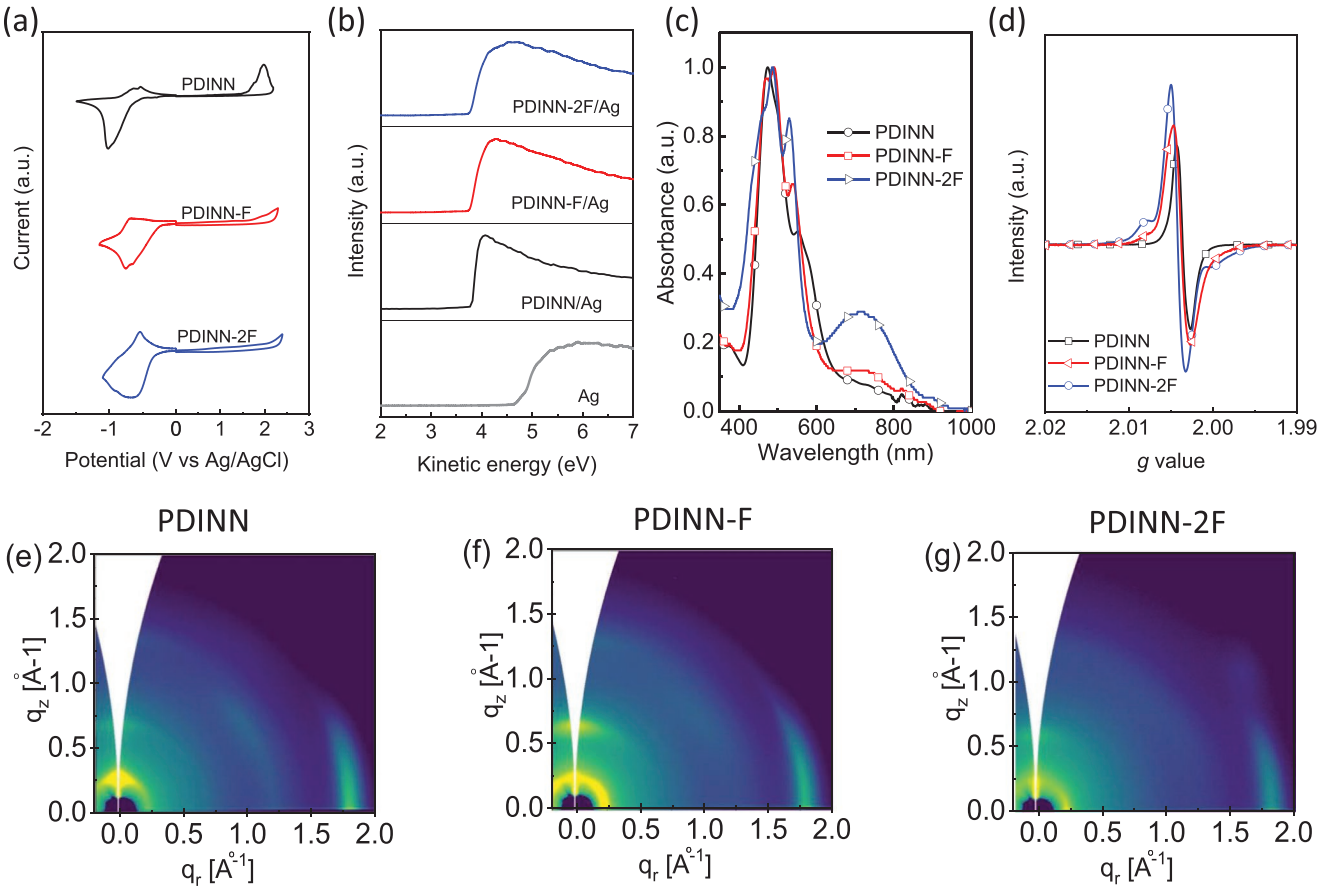

Figure 2. a) Cyclic voltammograms of PDINN and its fluorinated derivatives. b) UPS spectra of the Ag electrodes covered with different PDI CILs. c) Normalized film absorptions of the PDI CILs. d) Solid-state ESR spectra of the PDI CILs. e–g) 2D GIWAXS diffraction patterns of the thin films of PDINN (e), PDINN-F (f), and PDINN-2F (g).

Information, the fluorine substituent on the bay area of the PDI core greatly decreased their LUMO energy levels. In addition, the fluorine substitution enhances the electronegativity of the PDI core and leads to a decreased surface electrostatic potential (ESP), which will improve their electrostatic attraction with the acceptor (with a strong positive ESP value).[43] Therefore, the fluorination of the PDINN derivatives is favorable for electron extraction from acceptors in the active layer.

2.2. Photophysical Properties

Cyclic voltammetry measurements were performed to experimentally estimate the LUMO energy level (E_{LUMO}) and HOMO energy level (E_{HOMO}) of the PDIs. **Figure 2**a shows the cyclic voltammograms of the PDI derivatives, from which the onset oxidation/reduction potentials ($\varphi_{ox/red}$) were obtained. According to the equation $E_{LUMO} = -e(\varphi_{red} - \varphi_{Fc^+/Fc} + 4.8)$ (eV), the E_{LUMO} values were calculated as −3.78, −4.08, and −4.00 eV for PDINN, PDINN-F, and PDINN-2F, respectively (**Table 1**). The fluorinated derivatives show relatively lower LUMO energy levels, which confirms the predicted influence of fluorination on the PDI core. The LUMO energy levels of PDINN-F and PDINN-2F are very close to that of the NIR-absorbing acceptors, which would lead to better energy level alignment at the cathode interface and, thus, improve the energy landscape for electron extraction. From cyclic voltammograms, the E_{HOMO} values of the three PDIs are −6.02, −6.05, and −6.06 eV for

Table 1. Comparison of the photophysical properties of PDINN, PDINN-F, and PDINN-2F.

	Film absorption [nm]		ε,[a)] [10^4 M^{-1} cm^{-1}]	LUMO [eV]	HOMO [eV]	WF of Ag with CIL [eV]
CILs	λ_{max}	λ_{edge}				
PDINN	473	630	2.30	−3.78	−6.02	3.72
PDINN-F	490	600	2.27	−4.08	−6.05	3.78
PDINN-2F	486	580	1.90	−4.00	−6.06	3.77

[a)]solution absorbance

PDINN, PDINN-F, and PDINN-2F, respectively. The low-lying E_{HOMO} values mean that these PDI-based CILs will sufficiently block holes from various donors (usually with E_{HOMO} of ≈−5.50 eV).

It is known that the WF-modifying ability of the CIL on the metal cathode is associated with the interfacial dipole of the CILs and plays a vital role in creating a built-in potential across the device.[11,44] With our interlayer on the metal electrode, an interfacial dipole is created by the donation of nitrogen lone pair electron of amine group of the CIL to the electrode and/or the permanent dipoles of ammonium. This dipole helps to establish ohmic contact between the organic layer and cathode through pinning the Fermi level of the cathode to a desirable position shallower than the quasi-Fermi levels of the active layer.[11] Ultraviolet photoelectron spectroscopy (UPS) was used to probe the WF values of the Ag cathode modified by the three PDIs, and the results are shown in Figure 2b. It can be seen that all of the PDIs effectively reduced the WFs of the Ag electrode, showing WF values of 3.72, 3.78, and 3.77 eV for PDINN, PDINN-F, and PDINN-2F, respectively. The slightly higher WF values of PDINN-F/Ag and PDINN-2F/Ag are due to the relatively small interfacial dipoles caused by their ammonium, which is consistent with Russell's results.[11] Anyway, the WF values of less than 3.8 eV for the PDINN-F and PDINN-2F-modified Ag electrode are low enough to form ohmic contact with active layer. The benefits of the two new fluorinated PDIs, including their suitable LUMO energy levels and strong WF-modifying ability, directly motivate us to utilize these materials as better CILs in efficient OSCs.

The UV–Vis absorption spectra of the three CIL films are displayed in Figure 2c, which shows the maximum absorption peaks at 473 nm for PDINN, 490 nm PDINN-F, and 486 for PDINN-2F. In solution, the molar extinction coefficient (ε) of the three PDIs was measured, showing a value of 2.30×10^4 M^{-1} cm^{-1} for PDINN, 2.27×10^4 M^{-1} cm^{-1} for PDINN-F, and 1.90×10^4 M^{-1} cm^{-1} for PDINN-2F (Figure S4, Supporting Information), the lower value for PDINN-2F may be ascribed to the twist of the PDI core when two fluorine atoms are added. For PDINN-2F, a distinct radical anion (polaron) feature is found in both solutions at 680 nm (Figure S4, Supporting Information) and film at 730 nm, which implies a self-doping effect.[45,46] While for PDINN-F, the self-doping effect indicated by the polaron absorption is largely weakened and can only be observed in the solid-state. The doping effect was further verified by the electron spin resonance (ESR) spectroscopy, as shown in Figure 2d. All three samples show significant signals of self-doping behavior (*g* value of ≈2.0), which is enabled by the unpaired electrons in amine and/or the acetate anion in the polar group of PDIs and generally beneficial to improve the electrical conductivity of these materials.[16] Our result is in accordance with previous observations.[47] In our case, the lower LUMO energy level of PDINN-2F facilitates charge transfer thus the high intensity of the ESR signal is observed.

To elucidate both the crystallinity and texture formation (i.e., preferential orientation) of the PDI-based small molecules in their thin-films, we employed synchrotron-based grazing-incidence wide-angle X-ray scattering (GIWAXS) measurements (Figure 2e–g). The three PDI-based CILs exhibit a fairly polycrystalline structure due to the aggregation of the PDI core. The characteristic peaks of π–π packing (q = ≈1.8 $Å^{-1}$) at the in-plane direction imply that the three PDI molecules exhibit a preferred edge-on orientation with a π–π stacking distance of 3.5 Å.[48] The degree of crystallinity is progressively increasing from PDINN-2F to PDINN-F and to PDINN. Their corresponding π–π stacking crystalline coherence length was calculated (via Scherrer equation) to be 43.73, 51.6, and 52.2 Å, respectively (Figure S5, Supporting Information). We assume that the weakened crystallinity of PDINN-2F is due to the steric hindrance of the excess acetates attached to the polar chains.[49]

The electron mobilities of the PDI-based CILs were measured using an electron-only device structure, within the framework of the space-charge-limited current model. By fitting the *J*–*V* curves (Figure S6, Supporting Information), we estimated the electron mobilities of PDINN, PDINN-F, and PDINN-2F as 1.2×10^{-4}, 1.2×10^{-4}, and 8.0×10^{-5} cm^2 V^{-1} s^{-1}, respectively. In addition, we measured the electrical conductivity by depositing the PDI CILs on the two parallel silver electrodes. The conductivities of PDINN, PDINN-F, and PDINN-2F calculated from the *I*–*V* curves (Figure S7, Supporting Information) are 5.2×10^{-4}, 1.6×10^{-5}, and 1.1×10^{-6} S cm^{-1}, respectively. Thus, it is suggested that the electron mobility and conductivity of the three PDI-based small-molecular CILs are dominated by the morphology rather than the charge concentration in solid films. For PDINN-F, although a relatively weak molecule aggregation hinders the electron transport in film, PDINN-F exhibits a high enough electron-transport behavior as a CIL.

2.3. Photovoltaic Performance

To evaluate the effect of the fluorinated CILs on device performance, we fabricated conventional OSCs with a structure of indium tin oxide (ITO)/(poly(3,4-ethylenedioxythiophene): polystyrene sulfonate) (PEDOT:PSS)/PM6:BTP-eC9/CILs/Ag (**Figure 3**a). As for the active layer, PM6:BTP-eC9 blend represents the state-of-the-art photovoltaic blend (Figure S8, Supporting Information), in which BTP-eC9 is a typical NIR absorbing acceptor with a low LUMO energy level of –4.05 eV.[50] From Figure 3b, negligible energy offset between the LUMO level of the acceptor and the CIL is realized when the fluorinated interlayers are used, leading to a more favorable electron transport pathway.[17,30]

Current density–voltage (*J*–*V*) characteristics of the optimal OSCs with different CILs are compared in Figure 3c, and the relevant photovoltaic parameters are summarized in **Table 2**. The PDINN-based device exhibits a good efficiency of 17.50%, along with a V_{OC} of 0.839 V, a J_{sc} of 26.97 mA cm^{-2}, and an FF of 77.33%. Since PDINN-F delivers a more favorable electron transport pathway than PDINN, the FF and J_{SC} are improved to 78.23% and 27.39 mA cm^{-2}, respectively, and finally, the PCE of the OSCs based on PDINN-F is boosted to 18.02%. On the other hand, the PDINN-2F-based device shows a relatively lower PCE of 16.81%, resulted mainly from the loss in FF and J_{SC}. We preliminarily attribute this loss to the poor electric conductivity of PDINN-2F. Figure 3d shows the incident photon-to-converted current efficiency (IPCE) curves, and the integrated currents from the IPCE spectra match well with the J_{SC} values measured from the *J*–*V* curves. The PDINN-F-engineered device

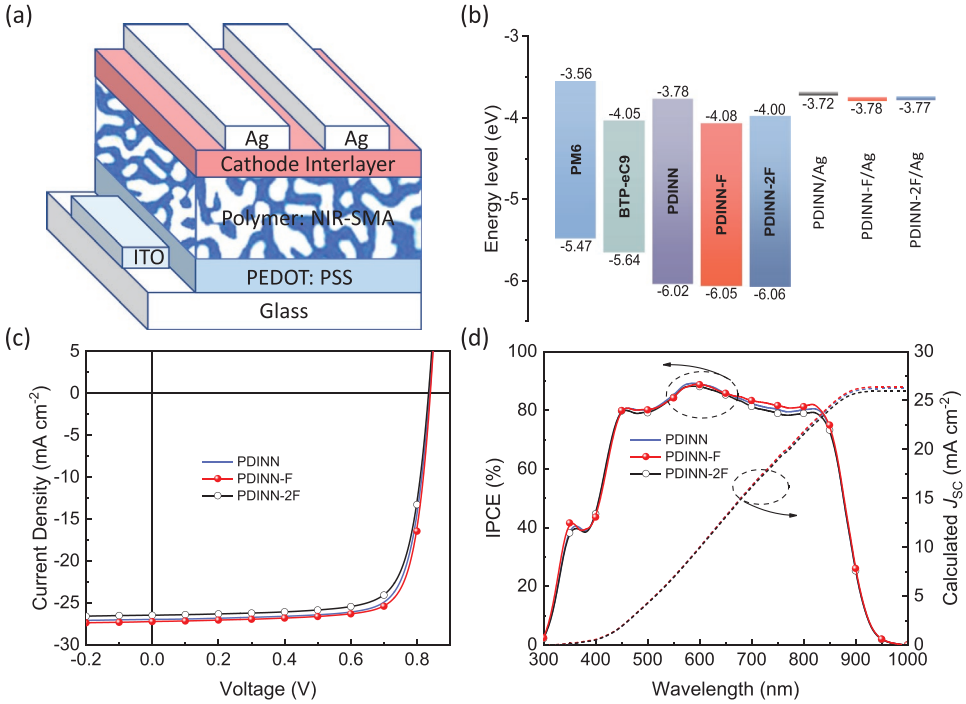

Figure 3. a) Device structure of the OSCs. b) Energy levels of PM6, BTP-eC9, PDINN, PDINN-F, and PDINN-2F, along with the WF of Ag electrodes modified by the CILs. c) *J–V* curves of the optimized OSCs under the illumination of AM 1.5G, 100 mW cm^{-2}. d) IPCE spectra and integrated current densities of the corresponding devices.

shows significantly higher IPCE response in the 650–850 nm range, which is the absorption from BTP-eC9. The higher IPCE in the acceptor absorption range indicates that PDINN-F can offer a more efficient electron extraction from the acceptor thus improving the photocurrent of the device. To support this, the electron-only devices of ITO/ZnO/BTP-eC9/CILs/Ag were fabricated, and the device based on acceptor/PDINN-F exhibited a higher current density (Figure S9, Supporting Information), suggesting a better electron extraction behavior relative to the devices based on PDINN and PDINN-2F.

We further investigated the film thickness sensitivity of three CILs on the photovoltaic performance of the OSCs. Commonly, the widely used PEIE and PFN CILs only work well at a critical thin thickness (<5 nm), where the electron can only tunnel through the CIL and be collected by the cathode. It is suggested this problem can be overcome with a desirable interfacial contact where the LUMO energy levels of CILs are below that of acceptors.[17] For the fluorinated derivatives, PDINN-F shows a better thickness-insensitivity due to its better matched LUMO energy level with respect to that of BTP-eC9, as highlighted in Figure S10 and Table S3, Supporting Information. Thus, it is beneficial for PDINN-F CIL to be used in the large-area device fabrication.

2.4. The Effect of Fluorinated CIL on Carrier Recombination of the OSCs

The charge recombination behavior of OSCs based on the three PDIs was further investigated. We studied the dependence of J_{sc} and V_{oc} on the light intensity (P), as shown in **Figure 4**a. In general, parameters J_{sc} and P follow the relationship of

Table 2. Photovoltaic performance of the OSCs based on PM6:BTP-eC9 with Ag as cathode and the PDINN derivative as CIL under the illumination of AM 1.5 G, 100 mW cm^{-2}.

Devices	V_{oc}[a)] [V]	FF[a)] [%]	J_{sc}[a)] [mA cm^{-2}]	PCE[a)] [%]	J_{sc} from IPCE [mA cm^{-2}]
PDINN	0.839	77.33	26.97	17.50	26.24
	0.834 ± 0.003	77.41 ± 0.34	26.67 ± 0.25	17.23 ± 0.26	
PDINN-F	0.841	78.23	27.39	18.02	26.40
	0.839 ± 0.003	77.60 ± 0.47	27.35 ± 0.10	17.80 ± 0.15	
PDINN-2F	0.835	76.18	26.43	16.81	25.97
	0.831 ± 0.004	75.86 ± 0.21	26.35 ± 0.09	16.60 ± 0.17	

[a)]Average value and standard deviation data are calculated from 10 devices.

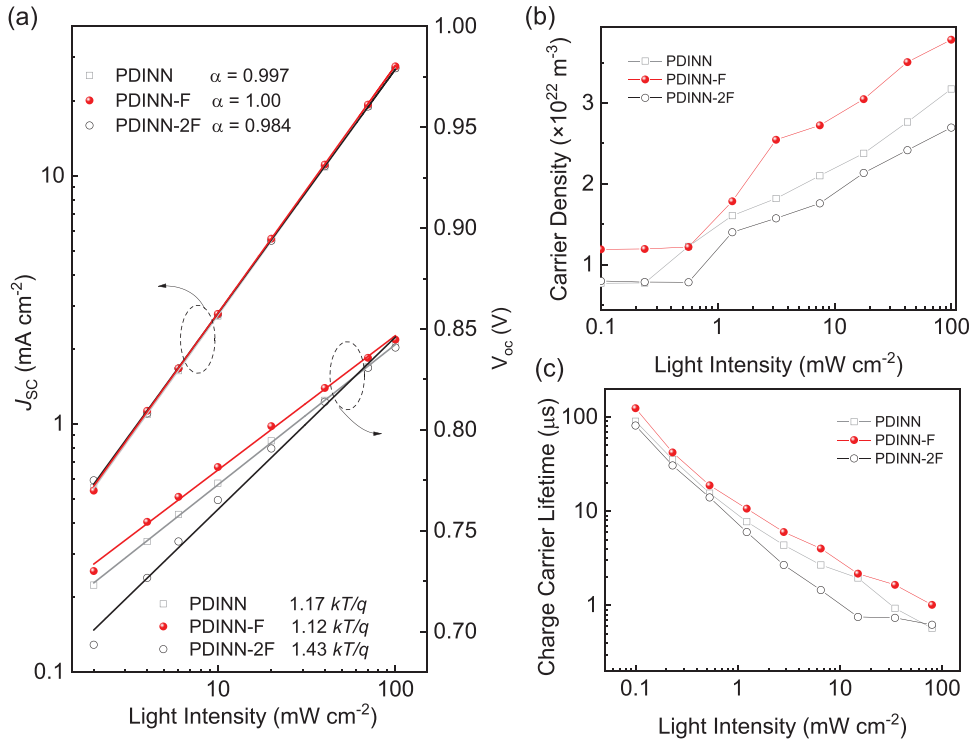

Figure 4. a) The dependence of J_{sc} and V_{oc} of the OSCs on the light intensity. b,c) The dependence of carrier density (b) and charge carrier lifetime (c) of the OSCs on the light intensity.

$J_{sc} \propto P^{\alpha}$.[51] The value of α should be 1 if the carriers are entirely extracted by the electrodes, while $\alpha < 1$ indicates some extent of bimolecular recombination. For the PDINN, PDINN-F, and PDINN-2F-based OSCs, the values of α are 0.997, 1.00, and 0.984, respectively. It is indicated that the PDINN-F-based device exists efficient transportation of carriers and negligible bimolecular recombination, which agrees well with the higher FF and J_{sc} value in the device. For the effect of V_{oc} on P, the competition between the bimolecular recombination and Shockley–Read–Hall type, trap-assisted recombination makes the slope of V_{oc} versus ln(P) between kT/q and $2kT/q$.[51] The devices using PDINN and PDINN-2F as CILs exhibit slopes of $1.17kT/q$ and $1.43kT/q$, while the device with PDINN-F CIL shows a slope of $1.12kT/q$, which is closer to kT/q, indicating the suppression of the trap-assisted recombination in the device.

Then, we investigated the charge carrier dynamics by exacting the carrier density (n) and charge carrier lifetime (τ) using charge extraction (CE) and transient photovoltage measurements, respectively, under different light intensity P. As shown in Figure 4b, the OSCs with PDINN-F show higher carrier density, which is in line with its higher J_{sc} value. A longer carrier lifetime was also detected in the PDINN-F-based device under different P conditions, as shown in Figure 4c. The bimolecular recombination rate constants (k_{rec}) can be obtained from the carrier densities and lifetime according to the equation of $k_{rec} = 1/((\lambda + 1)n\tau)$, where λ is the recombination order.[52] A lower k_{rec} value indicates the reduced recombination in the device. Since the k_{rec} is reciprocal to the product of n and τ, thus PDINN-F shows the smallest k_{rec} value among the samples. This implies that charge recombination is effectively suppressed in the PDINN-F-based device.

2.5. The Effect of Fluorinated CIL on Charge Transport of the OSCs

The exciton dissociation and charge collection properties of the OSCs with the three PDIs CILs were evaluated. **Figure 5**a shows the photocurrent density (J_{ph}) as a function of the effective voltage (V_{eff}) of the devices.[53] The photocurrent density J_{ph} is defined as $J_{ph} = J_L - J_D$, where J_L and J_D are the photocurrent densities under illumination and in the dark, respectively. The effective voltage V_{eff} is defined as $V_{eff} = V_0 - V_{bias}$, where V_0 is the voltage at which J_{ph} is zero and V_{bias} is the applied external voltage bias. The V_{eff} raises a suitable internal electric field in the device to suppress the charge recombination. In our case, the J_{ph} is saturated at V_{eff} of 1 V. The charge dissociation probability ($P(E,T)$) was estimated by the value of J_{ph}/J_{sat}, where J_{sat} represents the saturated photocurrent density. Under short circuit conditions, the ($P(E,T)$) values of the device with PDINN, PDINN-F, and PDINN-2F as CILs are 98.2%, 98.2%, and 98.1%, respectively. Furthermore, the photocurrent of the PDINN-F-based device is higher in the low-voltage range, which indicates that less driving force is needed to extract the carriers from the device.

Figure 5b shows J–V curves of the devices based on the three PDIs as CIL in the dark state. In the reverse bias region, the reverse saturation current of the PDINN-F-based device is the smallest among the three devices, indicating that PDINN-F effectively reduces the leakage current and internal charge loss by protecting the underlying active layer and eliminating pinholes and traps in it.[54] The result is also consistent with the highest FF and J_{sc} values of the device with PDINN-F CIL. In addition, the reverse saturation current reflects the number of

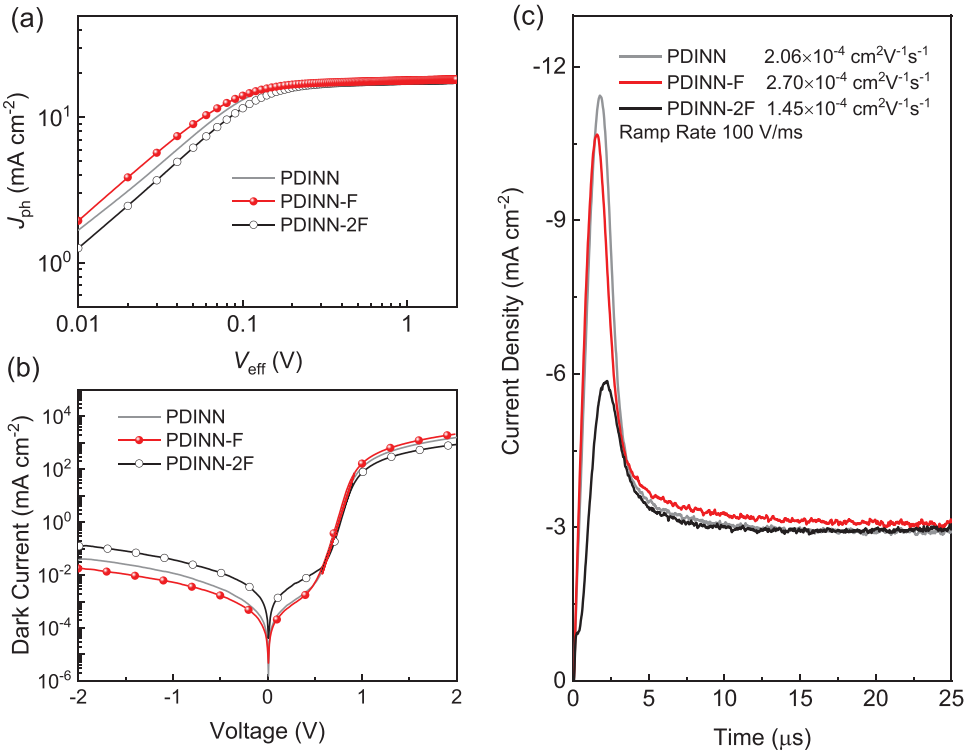

Figure 5. a) Plots of the photocurrent density versus effective voltage. b) *J–V* characteristic curves of the devices in dark state. c) Photo-CELIV traces of the devices.

charges (holes) that can overcome the energetic barrier in the reverse bias. Thus, the reduced reverse current densities of the PDINN-F-based device indicate the suppression of holes injection at the cathode interface. Under a positive bias, the current density of the PDINN-F-based device is higher than the other two devices due to smaller series resistance. As a result, the device shows a better rectification effect, which is beneficial to the reduction of the bypass leakage.

With the three PDI-based CILs, the carrier mobility in the OSCs was investigated using photoinduced charge-carrier extraction with linearly increasing voltage (Photo-CELIV; Figure 5c).[55] Transient current and characteristic features were recorded for calculating the mobility of the faster carrier component in the working OSCs with an equation: $\mu = 2d^2 / (3A - t_{max}^2 (1 + 0.36\Delta j / j_0))$, where d is the BHJ active layer thickness, A is the voltage rise speed of the applied voltage pulse, t_{max} is the time to reach the extraction current maximum, and Δj and j_0 are the shifting and initial current step, respectively. The device with PDINN-F CIL exhibits the highest charge mobility of 2.70×10^{-4} cm^2 V^{-1} s^{-1}, while the devices with PDINN or PDINN-2F CIL show relatively low mobility of 2.06×10^{-4} and 1.45×10^{-4} cm^2 V^{-1} s^{-1}, respectively. The measured mobility trend agrees with the recombination results discussed above. These results suggest that PDINN-F CIL facilitates the electron transport/extraction from the active layer.

2.6. Interfacial Contact and Morphology

The surface roughness of the CILs surface deposited on the PM6:BTP-eC9 active layer was evaluated by the atomic force microscopy (AFM, Figure S11, Supporting Information), showing a smooth surface with the root-mean-square roughness (R_q) values of 0.65 nm for PDINN and 0.94 nm for PDINN-F. The smooth surface of PDINN and PDINN-F can ensure a good interfacial contact to prevent defects when in contact with top metals. While, PDINN-2F exhibits a rough surface with an R_q value of 2.80 nm, which is rougher than the pristine active layer surface (R_q = 2.27 nm), thus degrading the performance of the device.

Meanwhile, the individual surface free energy of the active layer and the different CILs were calculated (Figure S12, Supporting Information) based on the Owens equation.[56,57] It can be seen that the active layer of PM6:BTP-eC9 shows a surface energy value of 19.1 mN m^{-1}. For PDINN, it shows an energy of 57.3 mN m^{-1} due to the polar group attached. It is well known that fluorination can decrease the surface energy, while with our fluorinated interlayer, they show significantly increased surface energies: a value of 61.2 mN m^{-1} for PDINN-F and 71.2 mN m^{-1} for PDINN-2F. This result suggests that amination dominated the surface energy of the interlayers. Generally, a solution of high free energy materials is unfavorable to wet and spread on the low surface energy solid. Hence, PDINN-2F with high surface energy hinders the uniformity of the interlayer, which is also confirmed by the AFM measurement. In addition, we calculated the interfacial energy of our CILs and PM6:BTP-eC9 active layer.[58] As shown in Table S4, Supporting Information, lower interfacial energies of 44.0 and 49.2 mN m^{-1} between the active layer and PDINN or PDINN-F CIL respectively indicate higher interfacial compatibility for the CILs and active layer, which is advantageous for PDINN and PDINN-F to form a uniform thin film on the surface of the active layer during the layer-by-layer solution deposition. However, the active layer with

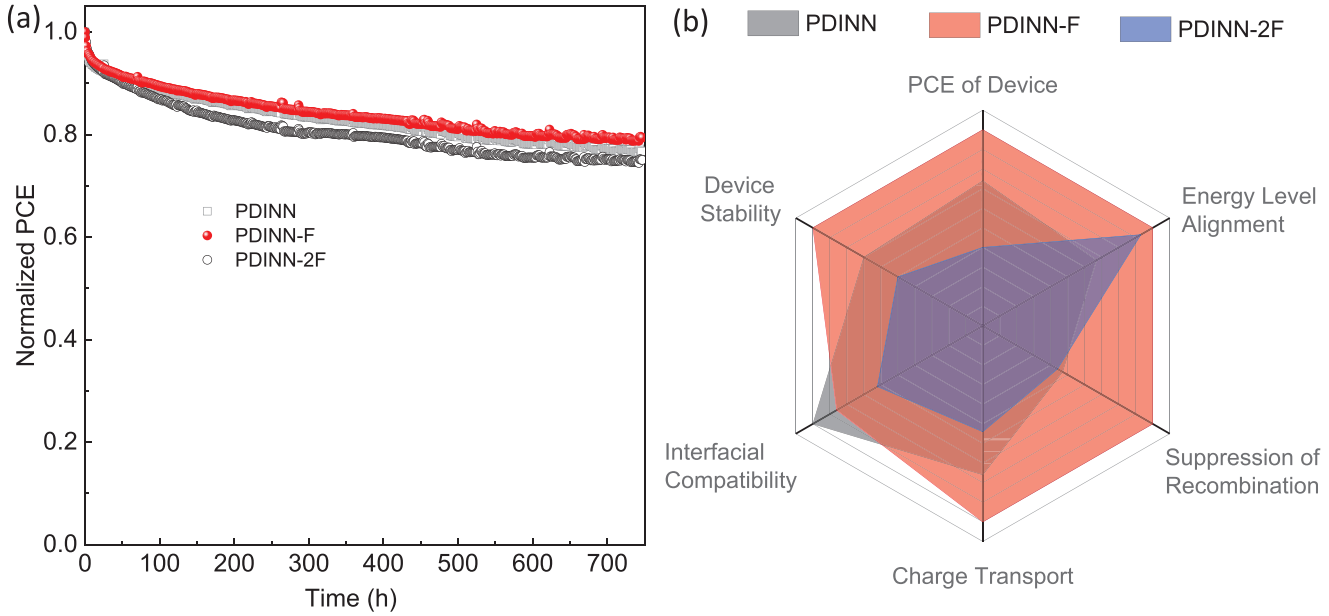

Figure 6. a) Normalized PCE plotted against aging time under 1-Sun illumination from white LED for representative devices. b) Radar chart for the comparison of the performance of three PDIs in various physical measurements.

PDINN-2F CIL showed a relatively higher interfacial energy value of 62.3 mN m^{-1}, indicating poor interfacial compatibility of PDINN-2F CIL with the active layer.

2.7. Stability

The long-term stability of the interlayer/electrode contact is an important issue that will directly impact the success of these materials and their OSC applications. Thus, we compared the device stability for the OSCs with the three PDI CILs. The devices were aged under 1-Sun equivalent illumination from white LEDs, continuously putting out current at the maximum power point which was calibrated by the measured *J–V* characteristic curves every hour. As shown in **Figure 6**a, the device with PDINN-F CIL maintained 80% of the initial PCE value after 750 h. While, the devices with PDINN and PDINN-2F CIL retained 77% and 75% of their initial PCE values, respectively. It is reported that PM6:BTP-eC9 blend is a thermodynamically unstable system,[59] thus the relaxation of the blend can cause the "burn-in" degradation for the devices. As for the difference in their degradation, the effect of CILs was taken into account. The relatively better stability of the PDINN-F-based devices is probably related to the suppressed trap-assisted recombination which usually induces so-called "burn-in" degradation in devices.[60] In addition, most of the PCE loss of our devices occurs during the first 50 h of aging, after which the tendency of decay slows, which is consistent with the report by Forrest et al.[61]

Finally, we systematically compared the advantages of these CILs in terms of device performance, energy level alignment at the cathode interface, suppression of charge recombination, electron extraction efficiency, interfacial contact, and the stability of devices, as shown in Figure 6b. PDIs that exhibit the best performance in each item will get full scores, and the other two get marks following the ratio to the best one. It is clear that PDINN-F shows advantages in almost all items, and the only less performance in interfacial contact is also good enough to form a smooth film for high efficiency in OSCs.

3. Conclusion

We have reported two new fluorinated PDI derivatives, PDINN-F and PDINN-2F, synthesized by the direct conversion of the aryl nitro to its fluorinated counterpart under mild reaction conditions within 15 min. The two bay-fluorinated PDI derivatives possess lowered LUMO energy level of ≈–4.0 eV, and PDINN-F also shows higher electron mobility. In the OSCs based on PM6:BTP-eC9 with PDINN-F as CIL, the matched LUMO energy level of the CIL with the BTP-eC9 acceptor removes the interfacial energy barrier on the cathode improves the electron extraction of the OSCs. Therefore, the OSCs based on PM6:BTP-eC9 with PDINN-F/Ag as the cathode, exhibited a high PCE of 18.02% with the enhanced FF and J_{SC}. Complimentary physical characterizations indicate that the high photovoltaic performance of the PDINN-F-based OSCs benefits from the suppression of charge recombination and the promotion of electron collection. In addition, the PDINN-F-based devices also achieved high stability, which represents an important advance toward future applications. Our results indicate that the fluorodenitration reaction is a mild, cost-effective, and scalable method for the preparation of fluorinated PDIs, and the proper fluorination on the CILs can both enhance the device efficiency and stability, making the NIR-SMAs-based OSCs more promising.

Acknowledgements

J.Y. and S.D. contributed equally to this work. The work was supported by the National Natural Science Foundation of China (Nos. 22175014, 21734008, and 51820105003), Fundamental Research Funds for the Central Universities (buctrc201822). Q.J.Z. thanks the NanHu Young Scholar Supporting Program of XYNU.The basic and Applied Basic Research Major Progrom of Guangdong Province (no. 2019B030302007). The authors thank the staff of the BL11 NCD-SWEET beamline at ALBA Synchrotron for their assistance in recording the GIWAXS data. J.A.S. acknowledges financial support from the Research Foundation – Flanders (FWO: grant No. 12Y7221N) and M.B.J.R. acknowledges support from the KU Leuven Research Fund (C14/19/079, iBOF-21-085 PERSIST), and the KU Leuven Industrial Research Fund (C3/19/046). The authors are thankful to Prof. Junfeng Xiang at Analysis and Test Ce

Keywords

cost-effective and scalable methods, fluorinated perylene-diimides, fluorination, high device performance

[1] G. Li, R. Zhu, Y. Yang, *Nat. Photonics* **2012**, *6*, 153.
[2] X. Ma, A. Zeng, J. Gao, Z. Hu, C. Xu, J. H. Son, S. Y. Jeong, C. Zhang, M. Li, K. Wang, H. Yan, Z. Ma, Y. Wang, H. Y. Woo, F. Zhang, *Natl. Sci. Rev.* **2021**, *8*, nwaa305.
[3] R. Sorrentino, E. Kozma, S. Luzzati, R. Po, *Energy Environ. Sci.* **2021**, *14*, 180.
[4] F. Li, A. K. Y. Jen, *Acc. Mater. Res.* **2022**, *3*, 272.
[5] Z. He, C. Zhong, X. Huang, W. Y. Wong, H. Wu, L. Chen, S. Su, Y. Cao, *Adv. Mater.* **2011**, *23*, 4636.
[6] F. Huang, H. Wu, D. Wang, W. Yang, Y. Cao, *Chem. Mater.* **2004**, *16*, 708.
[7] Y. Zhou, C. Fuentes-Hernandez, J. Shim, J. Meyer, A. J. Giordano, H. Li, P. Winget, T. Papadopoulos, H. Cheun, J. Kim, M. Fenoll, A. Dindar, W. Haske, E. Najafabadi, T. M. Khan, H. Sojoudi, S. Barlow, S. Graham, J. L. Bredas, S. R. Marder, A. Kahn, B. Kippelen, *Science* **2012**, *336*, 327.
[8] S. Xiong, L. Hu, L. Hu, L. Sun, F. Qin, X. Liu, M. Fahlman, Y. Zhou, *Adv. Mater.* **2019**, *31*, 1806616.
[9] F. Qin, W. Wang, L. Sun, X. Jiang, L. Hu, S. Xiong, T. Liu, X. Dong, J. Li, Y. Jiang, J. Hou, K. Fukuda, T. Someya, Y. Zhou, *Nat. Commun.* **2020**, *11*, 4508.
[10] X. Ouyang, R. Peng, L. Ai, X. Zhang, Z. Ge, *Nat. Photonics* **2015**, *9*, 520.
[11] Z. A. Page, Y. Liu, V. V. Duzhko, T. P. Russell, T. Emrick, *Science* **2014**, *346*, 441.
[12] C.-Z. Li, J. Huang, H. Ju, Y. Zang, J. Zhang, J. Zhu, H. Chen, A. K. Jen, *Adv. Mater.* **2016**, *28*, 7269.
[13] F. Pan, C. Sun, Y. Li, D. Tang, Y. Zou, X. Li, S. Bai, X. Wei, M. Lv, X. Chen, Y. Li, *Energy Environ. Sci.* **2019**, *12*, 3400.
[14] M. Cui, D. Li, X. Du, N. Li, Q. Rong, N. Li, L. Shui, G. Zhou, X. Wang, C. J. Brabec, L. Nian, *Adv. Mater.* **2020**, *32*, 2002973.
[15] Q. Kang, L. Ye, B. Xu, C. An, S. J. Stuard, S. Zhang, H. Yao, H. Ade, J. Hou, *Joule* **2019**, *3*, 227.
[16] Z. Wu, C. Sun, S. Dong, X. F. Jiang, S. Wu, H. Wu, H. L. Yip, F. Huang, Y. Cao, *J. Am. Chem. Soc.* **2016**, *138*, 2004.
[17] C. Sun, Z. Wu, Z. Hu, J. Xiao, W. Zhao, H.-W. Li, Q.-Y. Li, S.-W. Tsang, Y.-X. Xu, K. Zhang, H.-L. Yip, J. Hou, F. Huang, Y. Cao, *Energy Environ. Sci.* **2017**, *10*, 1784.
[18] Y. Qin, Y. Chang, X. Zhu, X. Gu, L. Guo, Y. Zhang, Q. Wang, J. Zhang, X. Zhang, X. Liu, K. Lu, E. Zhou, Z. Wei, X. Sun, *Nano Today* **2021**, *41*, 101289.
[19] C. Cai, J. Yao, L. Chen, Z. Yuan, Z. G. Zhang, Y. Hu, X. Zhao, Y. Zhang, Y. Chen, Y. Li, *Angew. Chem., Int. Ed.* **2021**, *60*, 19053.
[20] Z.-G. Zhang, B. Qi, Z. Jin, D. Chi, Z. Qi, Y. Li, J. Wang, *Energy Environ. Sci.* **2014**, *7*, 1966.
[21] M. Liu, Y. Jiang, D. Liu, J. Wang, Z. Ren, T. P. Russell, Y. Liu, *ACS Energy Lett.* **2021**, *6*, 3228.
[22] D. Zhou, W. You, F. Yang, R. Chen, H. Xu, Y. Tong, B. Hu, L. Hu, Y. Xie, L. Chen, *ACS Appl. Mater. Interfaces* **2021**, *13*, 50187.
[23] L. Nian, W. Zhang, N. Zhu, L. Liu, Z. Xie, H. Wu, F. Wurthner, Y. Ma, *J. Am. Chem. Soc.* **2015**, *137*, 6995.
[24] X. Wen, A. Nowak-Krol, O. Nagler, F. Kraus, N. Zhu, N. Zheng, M. Muller, D. Schmidt, Z. Xie, F. Wurthner, *Angew. Chem., Int. Ed.* **2019**, *58*, 13051.
[25] L. Nian, Z. Chen, S. Herbst, Q. Li, C. Yu, X. Jiang, H. Dong, F. Li, L. Liu, F. Wurthner, J. Chen, Z. Xie, Y. Ma, *Adv. Mater.* **2016**, *28*, 7521.
[26] J. Yao, Q. Chen, C. Zhang, Z. G. Zhang, Y. Li, *SusMat* **2022**, *2*, 243.
[27] S. Zhang, X. Ma, C. Xu, W. Xu, S. Y. Jeong, H. Y. Woo, Z. Zhou, X. Zhang, F. Zhang, *Macromol. Rapid. Commun.* **2022**, *43*, 2200345.
[28] M. Zhang, Y. Bai, C. Sun, L. Xue, H. Wang, Z.-G. Zhang, *Sci. China: Chem.* **2022**, *65*, 462.
[29] S. Chen, L. Liu, X. Gao, Y. Hua, L. Peng, Y. Zhang, L. Yang, Y. Tan, F. He, H. Xia, *Nat. Commun.* **2020**, *11*, 4651.
[30] L. Liu, S. Chen, Y. Qu, X. Gao, L. Han, Z. Lin, L. Yang, W. Wang, N. Zheng, Y. Liang, Y. Tan, H. Xia, F. He, *Adv. Mater.* **2021**, *33*, 2101279.
[31] D. Meng, R. Zheng, Y. Zhao, E. Zhang, L. Dou, Y. Yang, *Adv. Mater.* **2022**, *34*, 2107330.
[32] J. Yuan, Y. Zhang, L. Zhou, G. Zhang, H.-L. Yip, T.-K. Lau, X. Lu, C. Zhu, H. Peng, P. A. Johnson, M. Leclerc, Y. Cao, J. Ulanski, Y. Li, Y. Zou, *Joule* **2019**, *3*, 1140.
[33] X. Kong, J. Zhang, L. Meng, C. Sun, S. Qin, C. Zhu, J. Zhang, J. Li, Z. Wei, Y. Li, *CCS Chem.* **2022**, https://doi.org/10.31635/ccschem.022.202202056.
[34] Z.-G. Zhang, Y. Bai, Y. Li, *Chin. J. Polym. Sci.* **2020**, *39*, 1.
[35] R. Wang, J. Xu, L. Fu, C. Zhang, Q. Li, J. Yao, X. Li, C. Sun, Z. G. Zhang, X. Wang, Y. Li, J. Ma, M. Xiao, *J. Am. Chem. Soc.* **2021**, *143*, 4359.
[36] A. J. Gillett, A. Privitera, R. Dilmurat, A. Karki, D. Qian, A. Pershin, G. Londi, W. K. Myers, J. Lee, J. Yuan, S. J. Ko, M. K. Riede, F. Gao, G. C. Bazan, A. Rao, T. Q. Nguyen, D. Beljonne, R. H. Friend, *Nature* **2021**, *597*, 666.
[37] H.-L. Yip, A. K. Y. Jen, *Energy Environ. Sci.* **2012**, *5*, 5994.

[38] J. Yao, B. Qiu, Z. G. Zhang, L. Xue, R. Wang, C. Zhang, S. Chen, Q. Zhou, C. Sun, C. Yang, M. Xiao, L. Meng, Y. Li, *Nat. Commun.* **2020**, *11*, 2726.
[39] Y. Cho, H. R. Lee, A. Jeong, J. Lee, S. M. Lee, S. H. Joo, S. K. Kwak, J. H. Oh, C. Yang, *ACS Appl. Mater. Interfaces* **2019**, *11*, 40347.
[40] Y. Li, M. Han, W. Yang, J. Guo, K. Chang, J. Wang, J. Min, Q. Li, Z. Li, *Mater. Chem. Front.* **2019**, *3*, 1840.
[41] S. Caron, *Org. Process Res. Dev.* **2020**, *24*, 470.
[42] J. Tirado-Rives, W. L. Jorgensen, *J. Chem. Theory Comput.* **2008**, *4*, 297.
[43] Y. Xu, H. Yao, L. Ma, L. Hong, J. Li, Q. Liao, Y. Zu, J. Wang, M. Gao, L. Ye, J. Hou, *Angew. Chem., Int. Ed.* **2020**, *59*, 9004.
[44] Q. Chen, C. Wang, Y. Li, L. Chen, *J. Am. Chem. Soc.* **2020**, *142*, 18281.
[45] B. Russ, M. J. Robb, B. C. Popere, E. E. Perry, C. K. Mai, S. L. Fronk, S. N. Patel, T. E. Mates, G. C. Bazan, J. J. Urban, M. L. Chabinyc, C. J. Hawker, R. A. Segalman, *Chem. Sci.* **2016**, *7*, 1914.
[46] H. Guo, C.-Y. Yang, X. Zhang, A. Motta, K. Feng, Y. Xia, Y. Shi, Z. Wu, K. Yang, J. Chen, Q. Liao, Y. Tang, H. Sun, H. Y. Woo, S. Fabiano, A. Facchetti, X. Guo, *Nature* **2021**, *599*, 67.
[47] Z. Wang, N. Zheng, W. Zhang, H. Yan, Z. Xie, Y. Ma, F. Huang, Y. Cao, *Adv. Energy Mater.* **2017**, *7*, 1700232.
[48] Y. Xiao, X. Lu, *Mater. Today Nano* **2019**, *5*, 100030.
[49] D. Meng, H. Fu, C. Xiao, X. Meng, T. Winands, W. Ma, W. Wei, B. Fan, L. Huo, N. L. Doltsinis, Y. Li, Y. Sun, Z. Wang, *J. Am. Chem. Soc.* **2016**, *138*, 10184.
[50] Y. Cui, H. Yao, J. Zhang, K. Xian, T. Zhang, L. Hong, Y. Wang, Y. Xu, K. Ma, C. An, C. He, Z. Wei, F. Gao, J. Hou, *Adv. Mater.* **2020**, *32*, 1908205.
[51] A. K. Kyaw, D. H. Wang, V. Gupta, W. L. Leong, L. Ke, G. C. Bazan, A. J. Heeger, *ACS Nano* **2013**, *7*, 4569.
[52] C. G. Shuttle, B. O'Regan, A. M. Ballantyne, J. Nelson, D. D. C. Bradley, J. R. Durrant, *Phys. Rev. B* **2008**, *78*, 113201.
[53] D. J. Wehenkel, L. J. A. Koster, M. M. Wienk, R. A. J. Janssen, *Phys. Rev. B* **2012**, *85*, 125203.
[54] M.-H. Jao, H.-C. Liao, W.-F. Su, *J. Mater. Chem. A* **2016**, *4*, 5784.
[55] T. M. Clarke, C. Lungenschmied, J. Peet, N. Drolet, A. J. Mozer, *Adv. Energy Mater.* **2015**, *5*, 1401345.
[56] D. K. Owens, R. C. Wendt, *J. Appl. Polym. Sci.* **1969**, *13*, 1741.
[57] Y. Li, J. Ding, C. Liang, X. Zhang, J. Zhang, D. S. Jakob, B. Wang, X. Li, H. Zhang, L. Li, Y. Yang, G. Zhang, X. Zhang, W. Du, X. Liu, Y. Zhang, Y. Zhang, X. Xu, X. Qiu, H. Zhou, *Joule* **2021**, *5*, 3154.
[58] B. Lee, S. Kim, H. W. Nho, J. Oh, G. Park, M. Jeong, Y. Cho, S. M. Lee, O. H. Kwon, C. Yang, *Adv. Energy Mater.* **2021**, *11*, 2102594.
[59] M. Ghasemi, N. Balar, Z. Peng, H. Hu, Y. Qin, T. Kim, J. J. Rech, M. Bidwell, W. Mask, I. McCulloch, W. You, A. Amassian, C. Risko, B. T. O'Connor, H. Ade, *Nat. Mater.* **2021**, *20*, 525.
[60] H. Cha, J. Wu, A. Wadsworth, J. Nagitta, S. Limbu, S. Pont, Z. Li, J. Searle, M. F. Wyatt, D. Baran, J. S. Kim, I. McCulloch, J. R. Durrant, *Adv. Mater.* **2017**, *29*, 1701156.
[61] Q. Burlingame, X. Huang, X. Liu, C. Jeong, C. Coburn, S. R. Forrest, *Nature* **2019**, *573*, 394.